

# Finite Element Model of Mechanical Imaging of the Breast for OpenVCT Software Platform

Rebecca Axelsson  
Lund, June 2020



**LUND**  
UNIVERSITY

Master's Thesis in  
Biomedical Engineering  
Faculty of Engineering, LTH  
Department of Biomedical Engineering  
Supervisors: Predrag Bakic, Magnus Dustler,  
and Hanna Isaksson

# Acknowledgements

I would like to thank my supervisors Magnus Dustler, Predrag Bakic and Hanna Isaksson for their support, guidance, and insight through this master thesis project. It has been great working together with you and I have learnt a lot.

Thank you also to the LUCI-group in Malmö for your warm welcome and making me feel included in all we have done together.

## Major contributions

The overarching concept of the thesis was to introduce mechanical imaging to the *OpenVCT* software platform. The planning was done with all supervisors together with the author. The effort of this was built upon the *OpenVCT* (Barufaldi et al., 2018) software, and the meshing of the breast phantoms by Oliver Diaz. The framework for simulating mammographic compression of a breast phantom originates in the study by Lago et al. (2013).

The presented work resulted in a preliminary computer model of the breast of MI acquisition which was not present in the *OpenVCT* pipeline before.

# Abstract

A change in stiffness of breast tissue is often connected to a pathological change. Some types of breast cancer such as infiltrating ductal carcinoma can be up to eight times stiffer than fat tissue. It has been found that during compression of the breast there will be a local area of relatively high stress at the breast surface at the location of a tumour. This type of mechanical imaging of the breast has been able to find cancers which can be difficult to find in mammography.

Virtual breast phantoms have been growing in number and complexity for the past couple of years. The breast models have been used to validate medical imaging modalities and their great advantage is their low computation time. Considering the advantage of using virtual breast phantoms and mechanical imaging, combining these two aspects could prove to be advantageous.

In this thesis a Finite Element model of a breast with a linear elastic material model was subjected to mammographic compression. A tumour was inserted to study the surface pressure values of the breast phantom. As a first step, it was tested how the simulated surface pressure matched the stress patterns seen with mechanical imaging on real breasts. The tumour's stiffness, size, and location was varied. For all simulated examples, a local area of relatively high stress at the location of the tumour was found. This is in agreement with available clinical data although on the lower end of the reported stress ranges.

# Sammanfattning

Styvhetsförändringar i bröstvävnad är ofta kopplade till en patologisk förändring. Vissa cancertyper som infiltrerande duktalt carcinom kan vara åtta gånger så styv som fettvävnaden runt omkring. Genom att komprimera bröstet och mäta trycket på bröstets yta har man identifierat att det blir en lokal förhöjning i tryck där det finns en tumör. Med hjälp av den här typen av mekanisk avbildning av bröstet har man kunnat hitta cancertumörer som kan vara svåra att hitta med mammografi.

Simulerade bröstfantomer har ökat både i antal och komplexitet de senaste åren. Bröstfantomen har använts för att validera medicinska avbildningssystem och den största fördelen med modellerna är den korta beräkningstiden. Med tanke på denna fördel av att kunna simulera många bröst på kort tid, samt fördelen med mekanisk avbildning hade det varit fördelaktigt att kombinera dessa två aspekter.

I detta projekt simulerades kompression av ett bröst med hjälp av Finita Element Metoden. En tumör lades till i bröstet för att undersöka om de simulerade resultaten av trycket i bröstet överensstämde med klinisk data. Tumörens styvhet, storlek och läge i bröstet varierades. I alla simulerade exempel identifierades lokala områden med högt tryck som överensstämde med tillgänglig klinisk data.

# Contents

<b>1</b>	<b>Introduction</b>	<b>1</b>
1.1	Purpose of the thesis . . . . .	2
<b>2</b>	<b>Background</b>	<b>2</b>
2.1	Anatomy of the breast . . . . .	2
2.2	Mammography . . . . .	3
2.3	Biomechanical properties of the breast . . . . .	4
2.4	Elastography . . . . .	5
2.5	Mechanical imaging . . . . .	6
2.5.1	Work on breast mechanical imaging by Dustler	6
2.6	Virtual Clinical Trials . . . . .	7
2.6.1	The OpenVCT software platform . . . . .	7
2.6.2	The breast phantoms of the OpenVCT-pipeline	8
2.6.3	The phantom deformer of the OpenVCT pipeline	9
<b>3</b>	<b>Theory</b>	<b>10</b>
3.1	Mechanics . . . . .	10
3.1.1	Stress . . . . .	10
3.1.2	von Mises stress . . . . .	10
3.1.3	Strain . . . . .	11
3.1.4	Young's modulus . . . . .	11
3.1.5	Linear elasticity . . . . .	12
3.1.6	Poisson's ratio . . . . .	12
3.2	Finite Element Method . . . . .	13
3.2.1	Number of elements in a mesh . . . . .	13
3.2.2	Convergence and convergence criteria . . . . .	14
3.3	PreView, FEBio, and the PostView software . . . . .	15
<b>4</b>	<b>Method</b>	<b>15</b>
4.1	Proof-of-principle with a simple geometry . . . . .	16
4.1.1	The meshing . . . . .	16
4.1.2	Material properties . . . . .	17
4.1.3	Boundary conditions . . . . .	17

4.2	The breast phantom of the <i>OpenVCT</i> pipeline . . . . .	18
4.2.1	Meshing the breast phantom . . . . .	19
4.2.2	Creating the model for mammographic compression of the breast . . . . .	20
4.2.3	Boundary conditions and material properties . . . . .	20
4.2.4	Creating a lesion in the breast phantom . . . . .	21
4.3	Improving the mesh and boundary conditions . . . . .	22
4.4	Evaluation of lesions . . . . .	22
<b>5</b>	<b>Results</b>	<b>25</b>
5.1	Proof-of-principle . . . . .	25
5.2	Effect of the stiffness of the lesion inside the breast . . . . .	26
5.3	Effect of the size of the lesion in the breast . . . . .	29
5.4	Effect of the location of the lesion along the chest wall . . . . .	31
5.5	Effect of the location of the lesion in the orthogonal directions to the compression plates . . . . .	33
<b>6</b>	<b>Discussion</b>	<b>36</b>
6.1	Limitations . . . . .	39
6.2	Clinical implementation and ethical aspects . . . . .	41
6.3	Future work . . . . .	42
<b>7</b>	<b>Conclusion</b>	<b>43</b>

# 1 Introduction

Breast cancer is the most common cause of death for women worldwide. Breast cancer accounts for 25% of all cancer cases affecting women (Stewart & Wild, 2014). In Sweden alone, there are 8000 cases of breast cancer every year (Bröstcancerfonden, 2019).

The rate of survival depends largely on when the cancer is detected. For this reason mammographic screening has been established in many countries worldwide (Gotzsche et al., 2013).

Despite the screening, not all cases of cancer detected, and some cancer tumours are missed. This is mainly because of unclear characteristics of the tumour or that it is too small to be detected (Garra et al., 1997).

A complement to mammographic breast screening which is currently being studied is mechanical imaging of the breast. Mechanical imaging involves applying force to an object to obtain information about its material properties (Sarvazyan et al., 2009).

Considering tumour tissue is stiffer than normal breast tissue, when the breast is compressed it has been shown that there will be relatively higher stress at the location of a tumour in comparison to the rest of the breast (Dustler et al., 2012)(Förnvik et al., 2013).

Since the early 2000s there have been studies regarding simulated virtual breasts (virtual breast phantoms). The simulated breasts are used in so-called "virtual clinical trials". Virtual clinical trials are simulations of clinical trials which can be used to validate different medical imaging modalities used in breast imaging, such as mammography and digital breast tomosynthesis (Vieira et al., 2013)(Young et al., 2013).

The strength of virtual clinical trials is their speed at which they can be run. Through virtual clinical trials it is possible to run a high number of simulations, which would have taken considerably longer than if it was done clinically (Bakic et al., 2018a).

Considering the results in detecting cancers from mechanical imaging and the advantage of virtual clinical trials, the combination of



these aspects could prove advantageous in finding cancer.

## 1.1 Purpose of the thesis

The purpose of this master's thesis is to introduce a mechanical imaging aspect to the *OpenVCT* software platform (Barufaldi et al., 2018), by considering the advantage mechanical imaging has in finding tumours that would otherwise remain undetected and most importantly whether a tumour is benign or not.

To use mechanical imaging on the current virtual breast phantoms, and considering we are interested in the local changes in pressure of the breast, a more complex mechanical model of the breast would be needed.

Additionally, the following questions are to be answered:

- How does the *location* of a lesion affect the stress at the surface of the breast phantom?
- How does the *stiffness* of a lesion affect the stress at the surface of the breast phantom?
- Does the *size* of the lesion affect the stress at the surface of the breast phantom?

## 2 Background

### 2.1 Anatomy of the breast

The breast consists mostly of glandular tissue and fat, surrounded by fibrous connective ligaments (Ramiao et al., 2016). The base of the breast attaches to the thorax through the pectorial fascia which is a sheet of connective tissue that in turn attaches to the pectorialis major.

The center of the breast and its upper portion is mainly glandular tissue which consists of ducts and secretory lobules which produces

milk. The lobes have excretory ducts that connect to the lactiferous sinus, which in turn connects to lactiferous ducts in the nipple and areola area. See figure 1.

The fibrous connective ligaments previously mentioned are called Cooper's ligaments and are a type of fibrous tissue that is fixed to the overlying skin and the underlying pectorial fascia of the breast. Cooper's ligaments aid in maintaining the internal structure and integrity of the breast (Vorrherr 1974, p. 26).

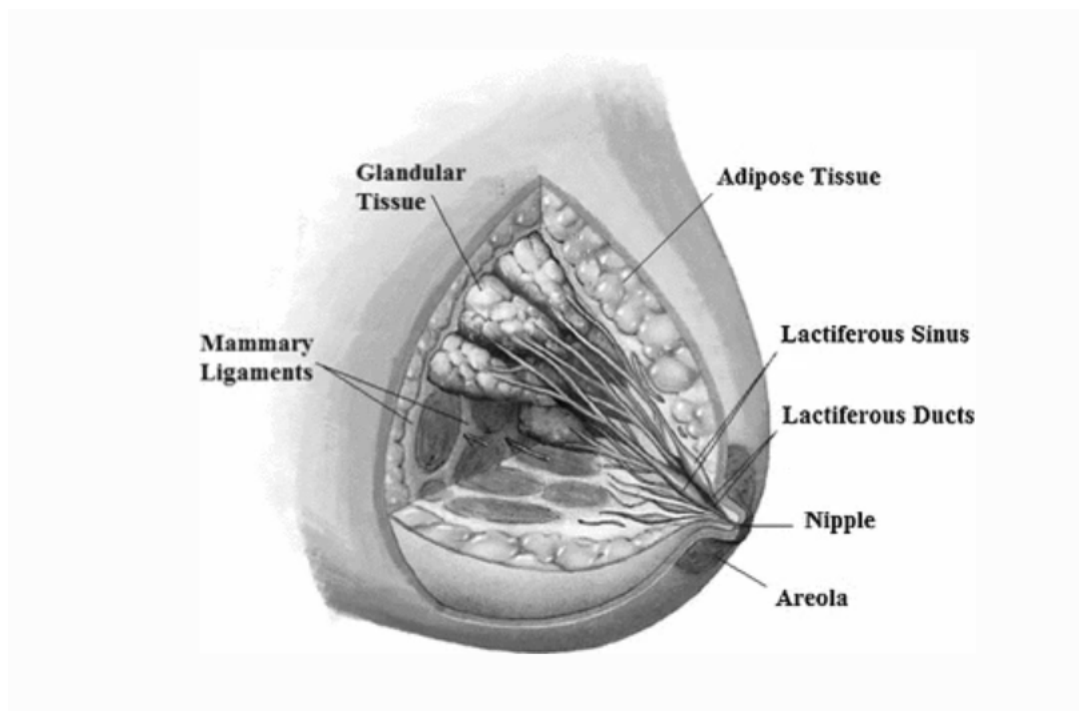


Figure 1: Anatomy of the breast. Adapted from Ramiao et al., 2016.

## 2.2 Mammography

Mammography is a medical imaging modality which uses X-rays in order to image the breast, mainly in order to detect cancers. Different

tissues will have different X-ray absorption and these small differences provide image contrast. Cancer can be detected by its characteristic shape and appearance.

There are two standard types of how the breast can be compressed, which is cranio-caudal (CC) and mediolateral oblique (MLO), see figure 2. Compression of the breast is done both to increase the image quality and reduce the amount of radiation absorbed by the patient.

In CC the breast is compressed horizontally (the transverse plane) while in MLO the breast is compressed laterally (the coronal plane) and the plates can be rotated between  $45^{\circ}$ - $55^{\circ}$ . Both views complement each other as CC provides with visualization of the central part of the breast and have less overlap of dense tissue while MLO provides with better juxta-thoracic imaging.

During a mammography examination the breast is placed between what is called a "breast support" and a compression plate. The breast support is fixed while the compression plate will compress the breast. The breast is compressed roughly to 50% of its original thickness. After this an X-ray image of the breast is taken (Andersson et al., 1978),(Kim et al., 2006),(Curry et al., 1990).

### **2.3 Biomechanical properties of the breast**

In a study done by Krouskop et al. (1998) the mechanical properties of fat, glandular tissue, fibrous tissue, invasive ductal carcinoma and intraductal carcinoma was investigated.

It was found that the elastic modulus of fat did not change with strain level, whereas the glandular tissue's elastic modulus increased with increasing strain. As was the case for fibrous tissue.

Both the intraductal carcinoma and the invasive ductal carcinoma were significantly stiffer than other tissues. Especially invasive ductal carcinoma had a higher elastic modulus than any other type of tissue tested.

Moreover, already in 1953 Andersson et al. showed that a change in stiffness in tissue is connected to a pathological change. In another

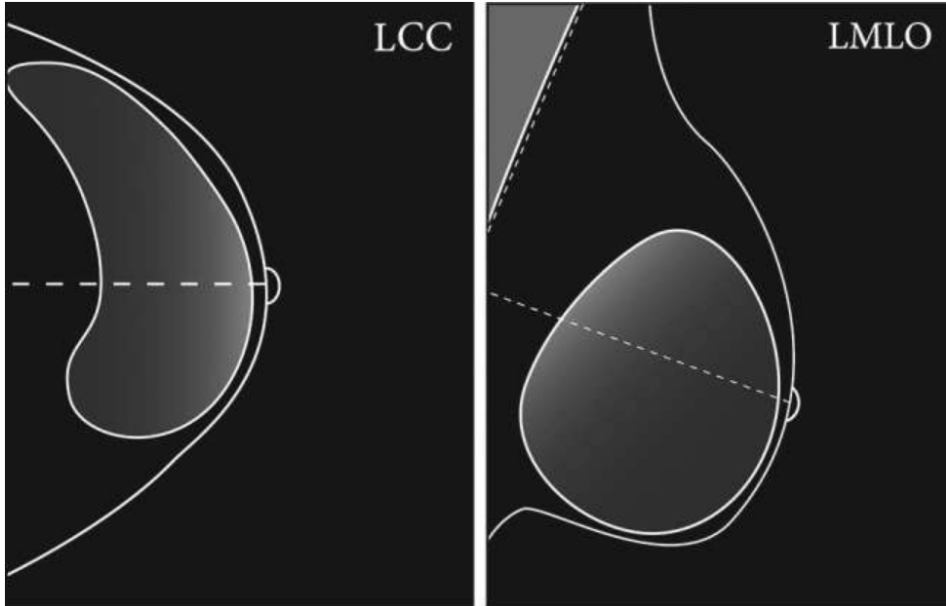


Figure 2: Image of the two standard types of mammographic view. On the left is cranio-caudal (CC) to the right is mediolateral oblique (MLO). MLO can be compression of the breast between  $45^{\circ}$ - $55^{\circ}$ . The "L" in both images signifies it is the left breast which is being compressed. Adapted from Sweeney et al., 2018.

study by Sarvazyan (1993) it was shown that fibroadenoma on average was four times stiffer than normal tissue and Waltz et al. (1993) showed that fibroadenoma could be eight times less stiff than carcinoma. In other words, benign tumours such as fibroadenoma are less stiff than malign tumours such as carcinoma.

## 2.4 Elastography

Elastography is the science of procuring an image displaying the mechanical properties of tissue (Ophir et al., 1996). This is done by adding compression to the tissue and recording the resulting radiofre-

quency (using ultrasound). The radiofrequency in this case is a small quasi-static compressive force. The radiofrequency is recorded both before and after compression. From this the axial strains can be estimated and the resulting image that is called an elastogram, shows the relative change in strain for an object as it is compressed. The elastogram can then be compared with images from for example ultrasound to find lesions that would otherwise not have been detected.

For example, in ultrasound examination when lesions are too similar from a echogenic perspective (ability of the tissue to echo back) to the surrounding tissue, they are difficult or even impossible to detect (Hricak, 1995)(Garra et al., 1997). As elastography measures the relative strain of the tissue, it becomes apparent as the tumors are stiffer than the surrounding normal tissue (Ophir et al., 1996)(Belaid et al., 1994).

## **2.5 Mechanical imaging**

Mechanical imaging involves determining the mechanical properties in a body as it is subjected to a determined force. The properties can be acquired by for example compressing the object and record the mechanical stress (Sarvazyan, 2009).

### **2.5.1 Work on breast mechanical imaging by Dustler**

In a study by Dustler et al. (2017) it was shown that mechanical imaging could be used to discern malignant tumours from benign tumours and is mechanical imaging's greatest advantage.

A total of 155 women took part in the study, all who had been recalled from mammography screening. It was shown that by measuring the local pressure in the breast during mammographic compression malignant tumors could be discerned from benign by using the Relative Mean Pressure on lesion Area (RMPA) of the tumour.

The median RMPA was 3.0 in the case of malignant tumors (biopsy proven), 1.3 for benign tumors which were biopsy proven and 1.0 for

tumours which were not biopsy proven. The differences were significant ( $p < 0.0001$ ).

## 2.6 Virtual Clinical Trials

Virtual clinical trials, in short VCT, are computer generated simulations of clinical trials. The entire process of a clinical trial can be simulated and everything that it entails: acquisition of data from patients, processing of images or other relevant data, readers interpreting the data, etc. VCTs can also be tailored to a number of purposes depending on what is needed; if only a certain part of a clinical trial is of interest then specifically that part can be simulated (Bakic and Maidment, 2012)(Diekmann et al., 2009).

Specifically for VCTs concerning breast imaging, breast phantoms are generated as to simulate the breast of a virtual patient. If for example a mammography procedure was simulated in a VCT, first a breast phantom would be generated and then subjected to simulated compression. The deformed breast phantom would be used to create the corresponding X-ray image of the phantom. The necessary image processing of the X-ray images would be done to get a fully processed X-ray image of the breast phantom, and possibly read by virtual readers (Maidment, 2014).

### 2.6.1 The OpenVCT software platform

The open source software platform *OpenVCT* (Barufaldi et al., 2018) was developed at University of Pennsylvania, and is a pipeline consisting of a number of simulations modules. Each module is a specialized part, from generating a breast phantom to having a virtual reader (in this case a virtual radiologist) scrutinize the generated mammogram from the breast phantom, as it would have been done in a real clinical trial. See figure 3 for the full *OpenVCT* pipeline.

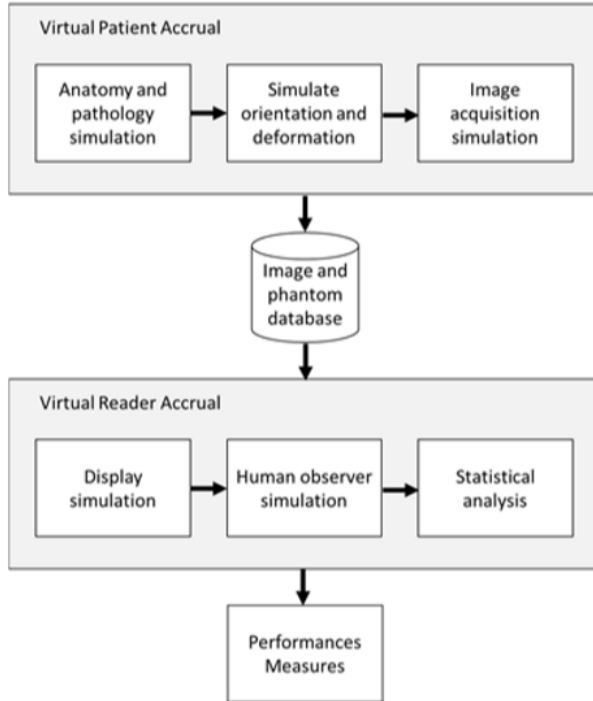


Figure 3: Flowchart of the full pipeline of the *OpenVCT* software platform. Adapted from Barufaldi et al., 2018.

### 2.6.2 The breast phantoms of the OpenVCT-pipeline

In a study done by Bakic et al. (2018a) breast phantoms were created by using an octree-based recursive partitioning method originating in Pokrajac et al. (2012). The user chooses the size of the breast, whether it has lesions or not, size of the lesions, amongst other input parameters.

The breast phantom is divided into three different regions depending on tissue: the subcutaneous, interior and retromammary, see figure 4. Both the subcutaneous (the anterior part of the breast) and retromammary (the deeper part of the breast, closest to the chest wall)

regions usually consist of compartments of relatively large size and are mainly labelled adipose tissue (fat tissue). The interior region of the breast consists of smaller compartments which are mostly labelled as glandular tissue. Overall the breast is built up by several types of tissue such as skin, adipose tissue, fibrous ligaments, and fibroglandular tissue, as well as lesions.

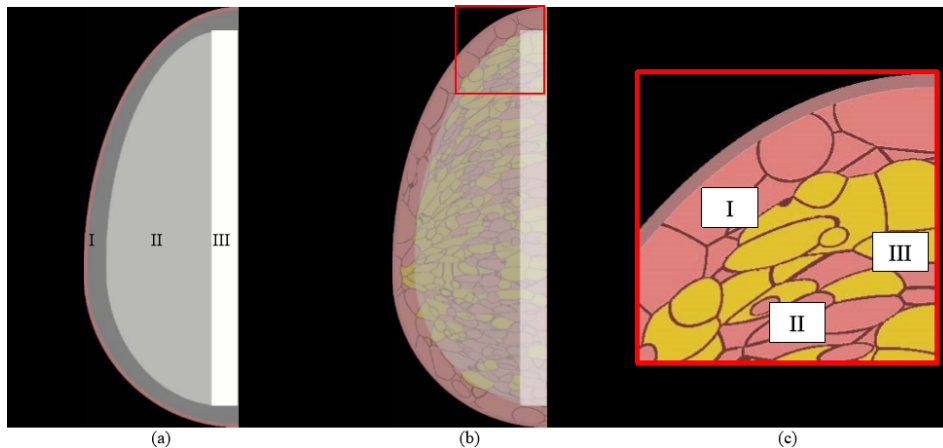


Figure 4: (a) Virtual breast phantom generated in the *OpenVCT* phantom generation pipeline. I is the subcutaneous part of the phantom, II the interior and III the retromammary. (b) The same breast phantom with compartments of labelled tissue belonging to each part. (c) A close-up, marked by the red square in (b), where I-III show the different compartments in the phantom. Adapted from Bakic et al. (2018).

### 2.6.3 The phantom deformer of the *OpenVCT* pipeline

The phantom deformer in the *OpenVCT* pipeline uses the Finite Element Method to approximate how the breast phantom is deformed during compression. The breast phantom is resting on the fixed breast support and compressed by the compression plate, similarly as in



mammography. The solution is calculated through the usage of the Finite Element solver software *FEBio* (FEBio).

As for the mechanical properties of the breast phantom, a Neo Hookean material model was assumed for the entire breast. The Neo Hookean material model is used when modelling materials with hyper-elastic behaviour (Han et al., 2012). This approximation was done as the internal mechanical properties of the phantom was not the highest priority but rather that the computation time was decreased and as low as possible. The importance of having fast simulation is that a great amount of phantoms can be run in a relatively short amount of time (Lago et al., 2013).

## 3 Theory

### 3.1 Mechanics

#### 3.1.1 Stress

The definition of stress is the force per unit area of a material or object, see equation 1.

$$\sigma = \frac{F}{A} \quad (1)$$

where  $\sigma$  is the stress,  $F$  is the applied force on the body and  $A$  is the area upon which the force is applied.

The force in question can be both external forces in the case of a force applied to the outer surface of the object or internal forces coming from the material inside the object. Stress is measured in Pascal (Pa), with  $1 \text{ Pa} = 1 \text{ N}/\text{m}^2$  (Stähle 2015, p. 13).

#### 3.1.2 von Mises stress

The definition of von Mises stress is the stress that creates the same distortion energy as created by all combined applied stresses. See equation 2 for the von Mises stress defined in 3 dimensions:

$$\sigma_{VM} = \sqrt{\sigma_{xx}^2 + \sigma_{yy}^2 + \sigma_{zz}^2 - \sigma_{xx}\sigma_{yy} - \sigma_{yy}\sigma_{zz} - \sigma_{zz}\sigma_{xx}} + \sqrt{3(\tau_{xy}^2 + \tau_{yz}^2 + \tau_{zx}^2)} \quad (2)$$

where  $\sigma_{xx}$  is the stress in the x-plane,  $\sigma_{yy}$  the stress in the y-plane,  $\sigma_{zz}$  the stress in the z-plane,  $\tau_{xy}$  the shear stress in the xy-plane,  $\tau_{yz}$  the shear stress in the yz-plane and  $\tau_{zx}$  the shear stress in the zx-plane (Ford, 1963).

### 3.1.3 Strain

The definition of strain is the relation between an object's length before and after deformation. The equation for relative change in length of an object can be seen in equation 3 and the resulting strain is described by equation 4.

$$\frac{L_0 - l_0}{l_0} = \frac{u(x + \Delta x) - u(x)}{\Delta x} \quad (3)$$

$$\epsilon = \lim_{\Delta x \rightarrow 0} \frac{u(x + \Delta x) - u(x)}{\Delta x} = \frac{du}{dx} \quad (4)$$

where  $\epsilon$  is the strain,  $L_0$  is the length of the object after deformation and  $l_0$  is the original length of the object.

Strain is unitless (Stähle 2015, p. 2).

### 3.1.4 Young's modulus

Young's modulus, also called the modulus of elasticity, describes the relationship between stress and strain for a material, see equation 5.

$$E = \frac{\sigma}{\epsilon} \quad (5)$$

where  $E$  is the Young's modulus,  $\sigma$  is the stress and  $\epsilon$  is the strain. A material with a high Young's modulus would be a stiff material while a material with a lower Young's modulus would be a weaker material.

### 3.1.5 Linear elasticity

Elastic materials are defined as materials that will regain their original shape after deformation. In other words, the material will not permanently deform under force. A linear elastic material is defined by the equation:

$$\sigma = E\epsilon \quad (6)$$

where  $\sigma$  is the stress put on the material,  $E$  is Young's modulus and  $\epsilon$  is the strain of the material.

Depending on the material, it will only be elastic for a specific strain range. After this strain range is exceeded, the material is permanently deformed. Irreversible deformation is called plastic deformation (Krouskop et al., 1998).

### 3.1.6 Poisson's ratio

Poisson's ratio is the relation between the transverse strain and the axial strain in an object, see equation 7.

$$\nu = -\frac{d\epsilon_{trans}}{d\epsilon_{axial}} \quad (7)$$

where  $\nu$  is Poisson's ratio,  $\epsilon_{trans}$  is the transverse (perpendicular) strain and  $\epsilon_{axial}$  is the axial (parallel) strain. To clarify further,  $\epsilon_{trans}$  is the strain which is perpendicular to the direction of the force and  $\epsilon_{axial}$  is the strain which is in the same direction as the force.

The transverse strain,  $\epsilon_{trans}$ , is negative for tension along its own axis and positive for compression while the opposite is true for the axial strain. Poisson's ratio varies between the values  $-1 < \nu < 0.5$  for isotropic linear elastic materials. A negative Poisson's ratio would be a material like cork which collapses in on itself and shows minimal amounts of lateral expansion as it is compressed. A material which has a Poisson's ratio of 0.5 would be incompressible and deform elastically, such as adipose and glandular tissue which has a Poisson's ratio of  $\sim 0.5$  (Fung, 1993)(Gefen and Dilmoney, 2007).

## 3.2 Finite Element Method

The finite element method (FEM) is a method often used to solve mathematical and mechanical problems that can be described with differential equations.

The principle of FEM is to divide a region into a finite number of smaller, less complex compartments. These smaller parts are called "finite elements". Approximations that are valid for each element are made. Once the behaviour for each element has been determined, the elements can be summed together to give an approximation for the behaviour of the entire region. The geometry of all the elements together is called a "finite element mesh" (Ottosen and Petersson 1992, p. 1).

Between the elements are what are called "nodal points" where the variable can be assumed to have a certain value according to the specific approximation used (Ottosen and Petersson 1992, p. 2).

FEM solves problems by determining elements force and displacement at each nodal point. This is described by equation 8:

$$\mathbf{K}^e \mathbf{a}^e = \mathbf{f}^e \quad (8)$$

where  $\mathbf{K}^e$  is the element stiffness matrix,  $\mathbf{a}^e$  the nodal displacement vector for an element, and  $\mathbf{f}^e$  is the element force vector.

The general procedure of FEM is first to determine the stiffness of the elements, using the element's assumed material properties and equilibrium conditions. Using the derived the equilibrium equations for the problem, and the boundary conditions are enforced, and the system of equations for the problem are solved (Ottosen and Petersson 1992, p. 35).

### 3.2.1 Number of elements in a mesh

The number of elements in a model will determine how accurate the approximation/solution will be. This is logical as the more elements and in turn data points there are, a better approximation of the entire system/body can be done. The opposite is true for a coarser

mesh which has fewer elements (Ottosen and Petersson 1992, p. 2). However, a finer mesh comes with higher computational costs.

### 3.2.2 Convergence and convergence criteria

When elements become infinitely small the approximation will be infinitely close to the "real" solution, and this is what we call the "convergence criteria".

The convergence criteria has two requirements which needs to be fulfilled; completeness and compatibility, see equation 9.

$$\text{convergence criterion} = \text{completeness} + \text{compatibility} \quad (9)$$

Completeness refers to the fact that the approximation (the solution) to the problem must consist of both constant values and gradient values. Let's say that we have a body which has varying temperature field over it. With a coarse mesh, the temperature value for each value will vary more than in the case of a finer mesh when the elements are smaller. In the case when the elements are infinitely small, we either have that an element has a value of constant temperature or a constant gradient of temperature. It is from this that we get the completeness requirement.

Compatibility, also called the conforming requirement, is that the value in an element, eg. temperature, stress, must be continuous at the interface with its neighbouring elements.

The convergence criteria is not so strict as not to allow some relaxation of the requirements. Specifically, the compatibility requirement can be relaxed while the completeness criteria cannot.

When elements fulfill the compatibility (conforming) requirement they are called "confirming elements" and when this is not the case they are called "non-conforming elements" (Ottosen and Petersson 1992, p. 93).

### 3.3 PreView, FEBio, and the PostView software

PreView, FEBio and PostView are all free software developed at the University of Utah (research groups MRL and SCI) and Columbia University (research group MBL). The reason this software was used was that FEBio was already implemented into the *OpenVCT* pipeline.

PreView is a software which allows the user to create geometries, add a mesh to the geometry, establish boundary conditions and contacts, forces, and prescribed displacement on the object and how it should be solved. From PreView it is possible to export the created model into FEBio which will solve for the established problem.

FEBio is a FEM solver that can solve for solid, multiphase, fluid mechanics and heat transfer problems. FEBio was specifically created for solving problems in biomechanical engineering and can do both dynamic and quasi-static analyses. The input for FEBio is a so-called feb file which is a text file which can be created in two ways. The first way is to define the problem with the geometry, mesh, boundary conditions, etc. in PreView.

PostView is a software with which to view the results from FEBio. It is possible to view the solution graphically with animations of the problem (FEBio).

## 4 Method

Before modelling the compression of a breast phantom, the compression of a simpler geometry was simulated. This was to see even with a simpler model if we would get the expected mechanical behaviour. After this step, the breast phantom model was put through mammographic compression both with and without a lesion. With the inclusion of a lesion in the breast phantom it became difficult for the model to converge. The breast phantom was remeshed and had its boundary conditions changed. After this, using the new mesh and boundary conditions, the breast was compressed with the lesion stiffness, size and location being varied. See the flowchart in figure 5.

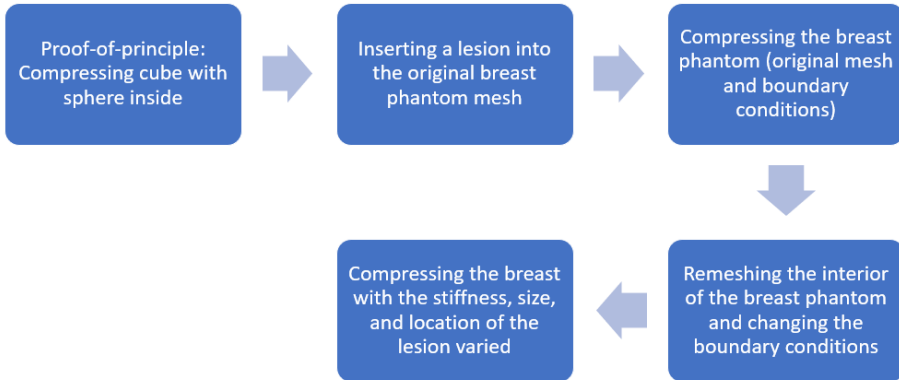


Figure 5: Flowchart of the overall methodology of the thesis.

## 4.1 Proof-of-principle with a simple geometry

In order to validate the principle of mechanical imaging for virtual breast phantoms, the first step was to simulate the compression of a 10x10x10 cm cube with a sphere inside the cube with a radius of 1 cm.

The reason for inserting a sphere was to see the effect that an internal structure would have on the top surface pressure of the cube as it was compressed. The cube was thus a first approximation of a breast while the sphere was an approximation of a lesion.

Three different examples were run; 1) the sphere had the same stiffness as the cube (in other words, a homogeneous cube), 2) the sphere was 10 times stiffer, and 3) the sphere was 100 times stiffer than the cube.

### 4.1.1 The meshing

Both the cube and the sphere were meshed separately by using the MATLAB toolbox "iso2mesh" (Fang and Boas, 2009). The element type for the mesh was tetrahedrals. The cube had 9651 elements and

the sphere had 3720 elements. After the meshes were created they were imported into PreView.

#### **4.1.2 Material properties**

The material model used for the cube was linear elastic with a Young's modulus of 1000 Pa and a Poisson's ratio of 0.49. The sphere was also described with a linear elastic material model and had a stiffness from 1000 Pa (same stiffness as the cube), 10000 Pa (10 times stiffer than the cube), and 100000 Pa (100 times stiffer than the cube). The sphere had a Poisson's ratio 0.49 for all examples.

#### **4.1.3 Boundary conditions**

See figure 6a for the model geometry and the internal mesh in figure 6b. The cube's top surface had a prescribed negative displacement in the z-direction. The cube was compressed in the z-direction to roughly 40% of the its original size. The bottom surface of the cube was restricted in the z-direction.

The bottom of the cube was attached to a 15x15x1 cm rigid body which works to model the same scenario as when the breast is resting on the bottom compression plate in mammography. The rigid body was restricted in all directions.

The contact interface between the bottom surface of the cube and the rigid body was described with a "tied facet-to-facet" contact surface. The "tied facet-to-facet" means that the bottom surface of the cube and the top surface of the rigid body were connected to each other in such a way that they could not detach in the z-direction from one another.

The cube was labelled the "slave" while the rigid body was labelled the "master". The "slave" label means that these elements should give way to the movements/displacement of the "master" elements.

Another "tied facet-to-facet" contact interface was established between the cube and the sphere inside it. The cube was the "master" while the sphere was the "slave".



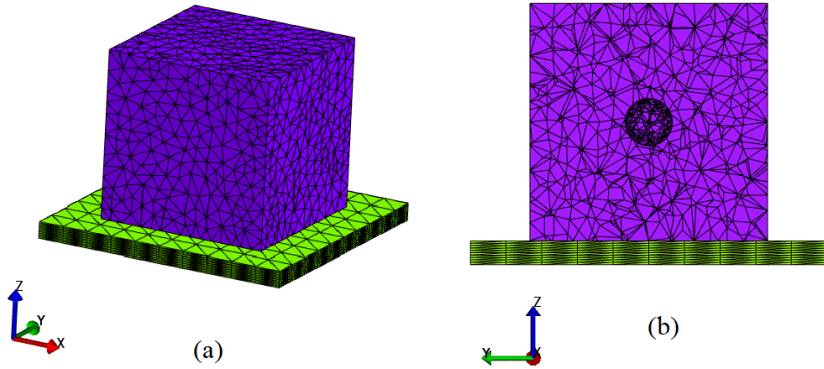


Figure 6: (a) Model of the cube with a sphere inside as viewed in PreView. In the coordinate system the blue arrow is the z-direction, red the x-direction, and green the y-direction. (b) Cut-through of the model in the x-direction.

The solver used was the "static" solver for problems in solid material mechanics. The deformation of the cube was prescribed over 1 s.

## 4.2 The breast phantom of the *OpenVCT* pipeline

After validating the results of the "proof-of-principle" examples, simulations of compressed breast phantoms with lesions were made.

For this thesis a pre-existing breast phantom from the *OpenVCT* pipeline was used as a starting point. The breast phantoms of the *OpenVCT* pipeline are ellipsoid in shape and have a certain width, height and length depending on the cup size that is generated. The breast size for the model was 170x75x37 mm.

### 4.2.1 Meshing the breast phantom

Using the images of the uncompressed breast phantom (378x188x851 pixels, where 378 was the length of the image, 188 the width, and 851 the number of slices), a volumetric mesh of the breast was created in MATLAB (code provided by Diaz) with "iso2mesh" MATLAB toolbox (Fang and Boas, 2009) using tetrahedral elements. After the mesh was created, it was saved as an .inp file.

The meshing parameters used were a maximum allowed element size for the mesh on the surface was 5 mm while the maximum element size for the interior elements was 300 mm. This resulted in a total of 61073 elements and 21274 nodes. See figure 7 for the surface mesh and figure 8 for the meshing inside the breast.

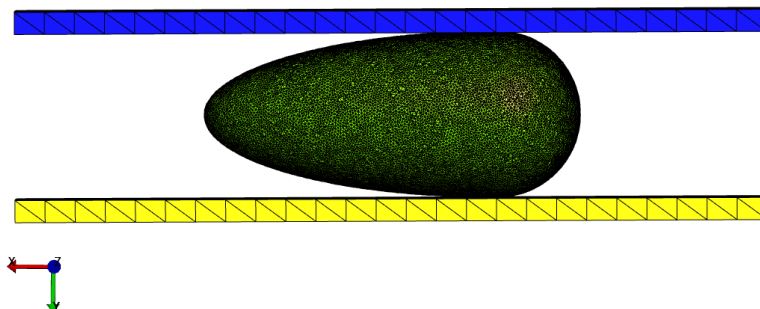


Figure 7: The surface for the breast phantom model as seen in PostView. The fixed breast support is in yellow while the moving compression plate is blue.

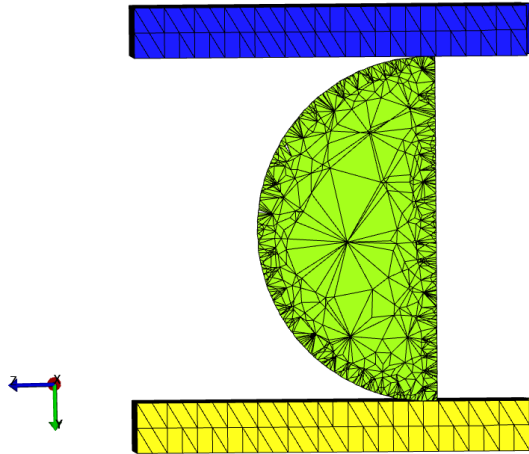


Figure 8: The mesh inside the breast phantom as seen in PostView, a cut-through in the x-direction. The fixed breast support is in yellow while the moving compression plate is blue.

#### 4.2.2 Creating the model for mammographic compression of the breast

The created .inp file, containing the information for all elements and nodes in the breast phantom mesh, was used as input in the MATLAB script "mainHomogenous.m" (Lago et al., 2013). Through "mainHomogenous.m" a .feb file was created which modelled the mammographic compression of a breast. The two plates, the boundary conditions, contacts between the breast and the plates, and material properties were all defined in the .feb file.

#### 4.2.3 Boundary conditions and material properties

The model had a breast support and a compression plate which were both defined as rigid bodies, see figure 7. The breast support was fixed in all directions while the compression plate was fixed in x and z but allowed to move in the y-direction. The compression plate was prescribed negative y-displacement of 3.76 cm. This corresponded to

the breast being compressed to 50% of its original thickness, as to emulate the case in mammography (Curry et al., 1990). The type of mammographic compression was MLO and was arbitrarily chosen.

The nodes of the breast which came into contact with the breast support were not restricted in any direction. The nodes at the top surface of the breast that came into contact with the compression plate were restrained in the x-direction (along the chest wall). Moreover, one node on the top surface was fixed to the compression plate in all directions to prevent the breast from detaching from the plate. The part of the breast which was towards the chest wall was restrained in the z-direction (nipple/areola direction), see the flat surface in figure 8.

Both plates' contact with the breast were defined as "facet-to-facet sliding", meaning no friction, with the plates being the "master" and the breast the "slave".

The breast was homogeneous, consisting entirely of fat tissue. It used a linear elastic material model and had a Young's modulus of 12750 and a Poisson's ratio of 0.49 (Han et al., 2012).

#### 4.2.4 Creating a lesion in the breast phantom

A script was written in MATLAB (see appendix, "lesion.m") to select an "area of interest" in the breast phantom's mesh where the lesion would be located.

The "area of interest" was defined as spherical to approximate the shape of a lesion. Both the center and radius of the sphere could be determined by the user. All nodes which were within the absolute distance in x, y, and z-direction equal or less to the radius from the origin were selected.

The reason for picking out nodes already belonging to the mesh itself instead of inserting an already meshed sphere into the breast was to reach the convergence criterion easier.

The selected nodes in the "area of interest" were matched to their corresponding element, where one element consists of four nodes (since the elements used were tetrahedrals). Those elements had

their material properties changed into the properties of the lesion (see "Onemesh.m" in appendix).

### **4.3 Improving the mesh and boundary conditions**

The initial reason for the coarse interior meshing was to make the simulation time as low as possible.

In the case of having a lesion in the breast, the expected results were not met and the model often failed to converge. This because of the mesh being non-conforming as the difference in size of the surface elements and the interior elements were large. Moreover, with the large and irregularly shaped interior elements, a spherical shape of the lesion was difficult to obtain.

Considering we were now interested in the mechanical properties and the stress at the surface of the breast, a finer mesh was needed both in order for the model to converge as well as provide with a higher accuracy result.

The model was remeshed in the same manner as previously. The maximum size of the interior elements was changed from 300 mm to 10 mm. The amount of elements in the new mesh was 172541 and 38360 nodes compared to the previous mesh which had 61073 elements and 21274 nodes. This resulted in doubling the simulation time.

The boundary conditions were also changed. When studying the x-displacement at full compression at the top surface of the breast, it was shown that the x-displacement was zero only in a certain region of where the breast was compressed. This resulted in high x-displacement in these areas as well as a local high stress, see figure 9. As more sliding behaviour was wanted, the boundary conditions were changed so that all nodes in contact with the upper compression plate were not restricted in any direction.

### **4.4 Evaluation of lesions**

The following eight examples were run with the new interior mesh and new boundary conditions. One parameter was varied at a time as to

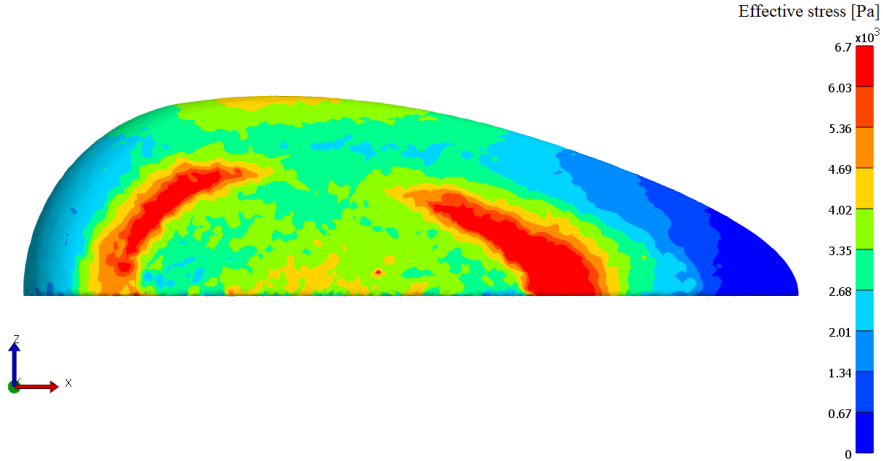


Figure 9: Breast phantom as viewed from the top in PostView at full compression. There is no lesion in the breast. The nodes of the upper surface of the breast that are in contact with the compression plate are restricted in the x-direction. The nodes of the chest wall are restricted in the z-direction.

see the effect of changing said parameter, see table 1.

The stiffness of the lesion was changed from being the same stiffness as the breast (Young's modulus 12750 Pa) and 50 times stiffer (Young's modulus 637500 Pa). For both examples the lesion 10 mm in diameter and located in the middle of the breast. The reason for choosing a large difference in stiffness between the examples was so the effect of increasing stiffness could be seen as clearly as possible.

The position of the lesion was varied in the x-direction (along the chest wall) by having one example of the lesion being 20 mm to the right and another 20 mm to the left.

The lesion was also varied in the y-direction, with the lesion being 20 mm in the positive y-direction (closer to the compression plate) and 20 mm in the negative y-direction (closer to the breast support).

The size of the lesion was also varied. The lesion was varied from a diameter of 15 to 22 mm.

For all examples pertaining the location and size of the lesion (in total six examples), the lesion had a diameter of 15 mm and a Young's modulus of 382500 (30 times stiffer than the background).

The lesion size was chosen from known sizes of invasive ductal carcinoma (Finlayson, 2000). This ranging from 5 mm to 50 mm. The size of the lesion being 10 mm and 15 mm was chosen arbitrarily while 22 mm was chosen because of the limits in size of the breast. Lesions with a diameter lower than 10 mm were also simulated, but were unable to be detected when studying the surface stress pattern of the breast.

The stiffness values chosen were based on the work of Krouskop et al. (1998) with ranges of stiffness for invasive ductal carcinoma at 20% precompression. The average stress value in this range had that the tumour was 30 times stiffer than the surrounding tissue while on the higher end of the range the tumour was 50 times stiffer.

The reason most examples had a lesion which was 30 times stiffer than the surrounding tissue was because this was the average reported stiffness by Krouskop et al. (1998).

Additionally, the average stress of the breast was calculated by taking the average of all stress values for all breast nodes. Also the average stress of a 3x3 cm square at the top surface of where the lesion was located. This was done in order to compare to Dustler's findings of "local hot spots" in earlier research studies (Dustler et al., 2012).

Also, the relative increase in stress was calculated. The relative increase in stress was the ratio between the average stress for the 3x3 cm patch and the average stress of the entire breast. This was also done in order to make it comparable to Dustler's work (Dustler et al., 2017).

Table 1: Examples run with the breast phantom with their respective diameter and Young’s modulus.

Example	Diameter (mm)	Young’s modulus (Pa)
Lesion x1	10	12750
Lesion x50	10	637500
Lesion 15 mm	15	382500
Lesion 22 mm	22	382500
Lesion left	15	382500
Lesion right	15	382500
Lesion up	15	382500
Lesion down	15	382500

## 5 Results

### 5.1 Proof-of-principle

It was found that for increasing stiffness of the sphere inside the cube, there was an increase in surface pressure at the top surface of the cube, see figure 10. Also the area of local high pressure at the top surface increased, gradually decreasing towards the edges of the cube.

For the homogeneous cube, the pressure throughout the cube and on its top surface (where it was compressed) varied little, see figure 10a.

In the case where the sphere was 10 times stiffer than the cube, there was a 10% increase in area of local high pressure at the top surface of the cube compared the homogeneous case, see figure 10b.

When the sphere was 100 times stiffer than the cube the area of local high pressure was increased 25% from the case with 10 times stiffness, see figure 10c.



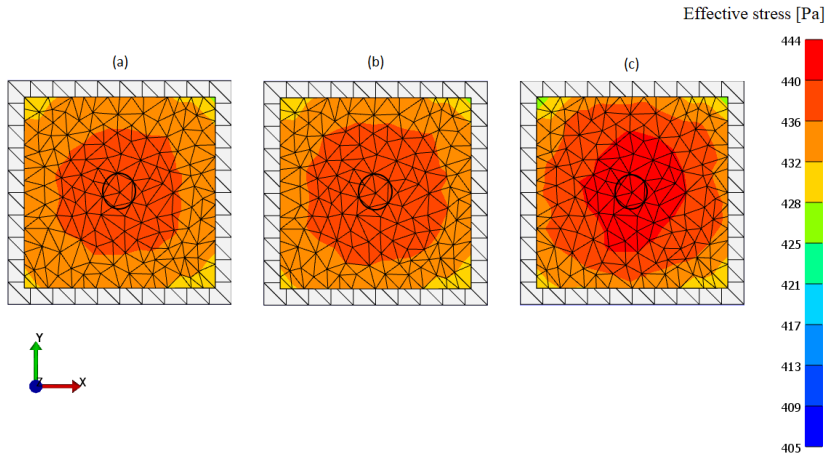


Figure 10: The effective stress (von Mises stress) at full compression, viewed from the top. The sphere was located in the middle of the breast with a radius of 1 cm. It is outlined by the circle seen on the surface of the cube. (a) The cube and the sphere had the same stiffness with a Young's modulus of 1000 Pa. (b) The sphere was 10 times stiffer than the cube. (c) The sphere was 100 times stiffer than the cube.

## 5.2 Effect of the stiffness of the lesion inside the breast

In the case where the lesion had the same stiffness as the breast, the stress was almost homogeneous over the breast. Gradually towards the edges of the breast, the part of the breast which was not under compression had lower stress than the part under compression. The average stress of the breast was 4141 Pa, see table 2 and figure 11a. The 3x3 cm square in the middle of the breast had an average stress of 4082 Pa.

The second example when the lesion was 50 stiffer there was a local increase in stress at the lesion's location, see figure 11b. The average stress of the breast was higher than the case with no lesions, with an

average stress of 4294 Pa and the average local maximum being 4860 Pa.

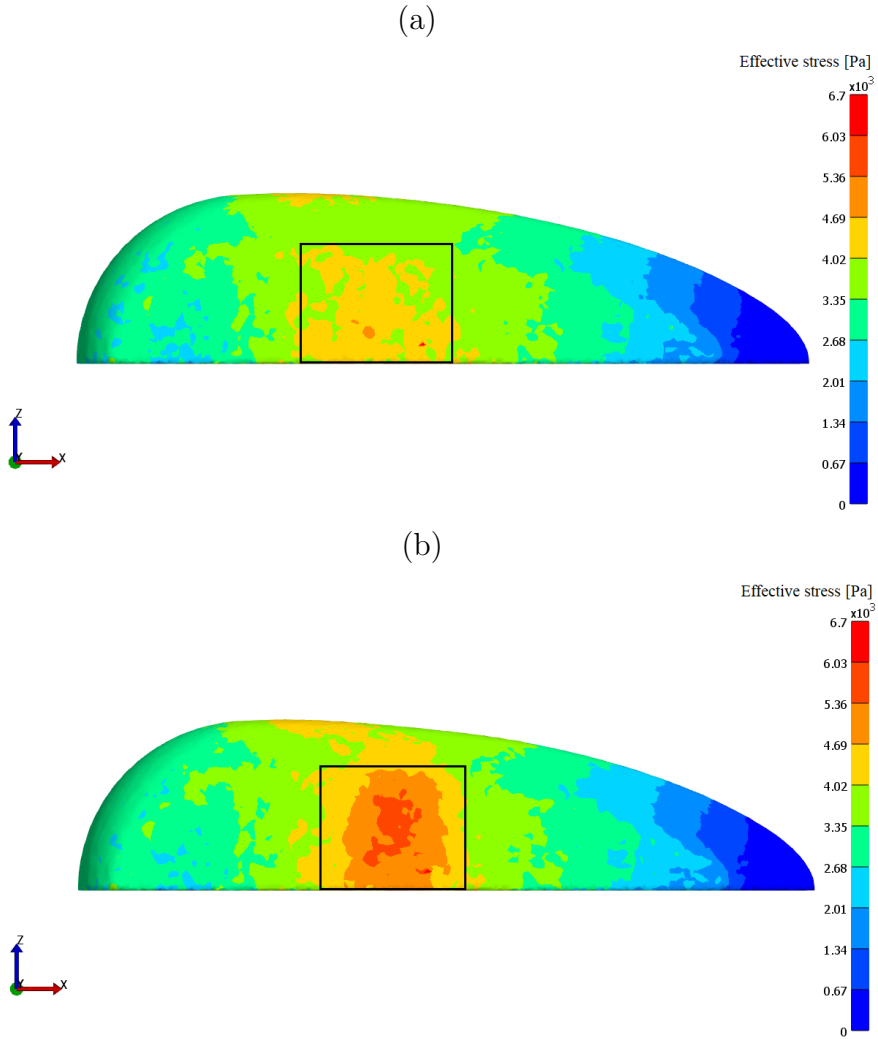


Figure 11: Both examples viewed from the top. (a) The breast phantom model with no lesions. The square outlines the 3x3 cm patch and is centered around the area of maximum stress. (b) The breast phantom model with lesion 10 mm in diameter located in the middle of the breast. The Young's modulus of the lesion was 50 times higher than the modulus of the surrounding tissue. The square outlines the 3x3 patch, centered on the lesion.

### 5.3 Effect of the size of the lesion in the breast

With increasing size of the lesion there was an increase in the local stress maximum at top surface of the breast at the location of the lesion. At 15 mm in diameter, see figure 12a, there was a higher local maximum stress at the location of the lesion while lower values around it. The average stress was 4765 Pa and the average for the local maximum was 5284 Pa, see table 2.

There was an increase in local maximum stress in the case of the lesion being 22 mm in diameter compared to the previous example, see figure 12b. Also the area of local high stress was bigger than in the previous example. There was a sharp border between the local maximum and the stress for the rest of the breast. Moreover, the shape of the breast changed due to the size of the lesion, buckling in slightly at the location of the lesion. The average stress was 4361 Pa and the local maximum 6412 Pa, see table 2.

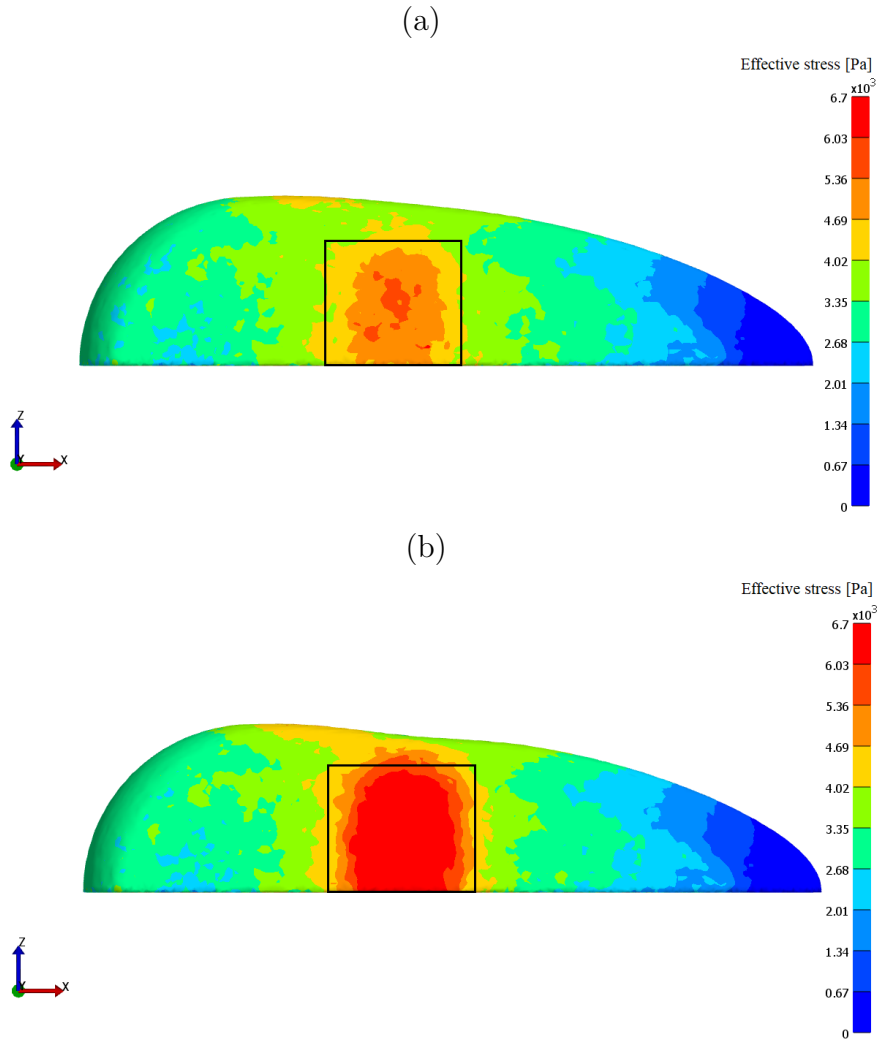


Figure 12: The lesion was 30 times stiffer than the surrounding tissue and was located in the middle of the breast. The square outline the 3x3 cm patch centered on the lesion. Viewed from the top. (a) The breast phantom model with a lesion 15 mm in diameter. (b) The breast phantom model with lesion located in the middle of the breast with a diameter of 22 mm.

## 5.4 Effect of the location of the lesion along the chest wall

In the case where the lesion was located 20 mm to the left along the chest wall, there was a local maximum of 4771 Pa (figure 13a). The average of the breast was 4236 Pa, see table 2. The area of local high stress was higher in comparison to when the lesion was placed on the right side.

The same behaviour could be seen when the lesion was located 20 mm to the right, with an average local stress maximum of 4497 Pa and an average stress of the entire breast at 4198 Pa (figure 13b).

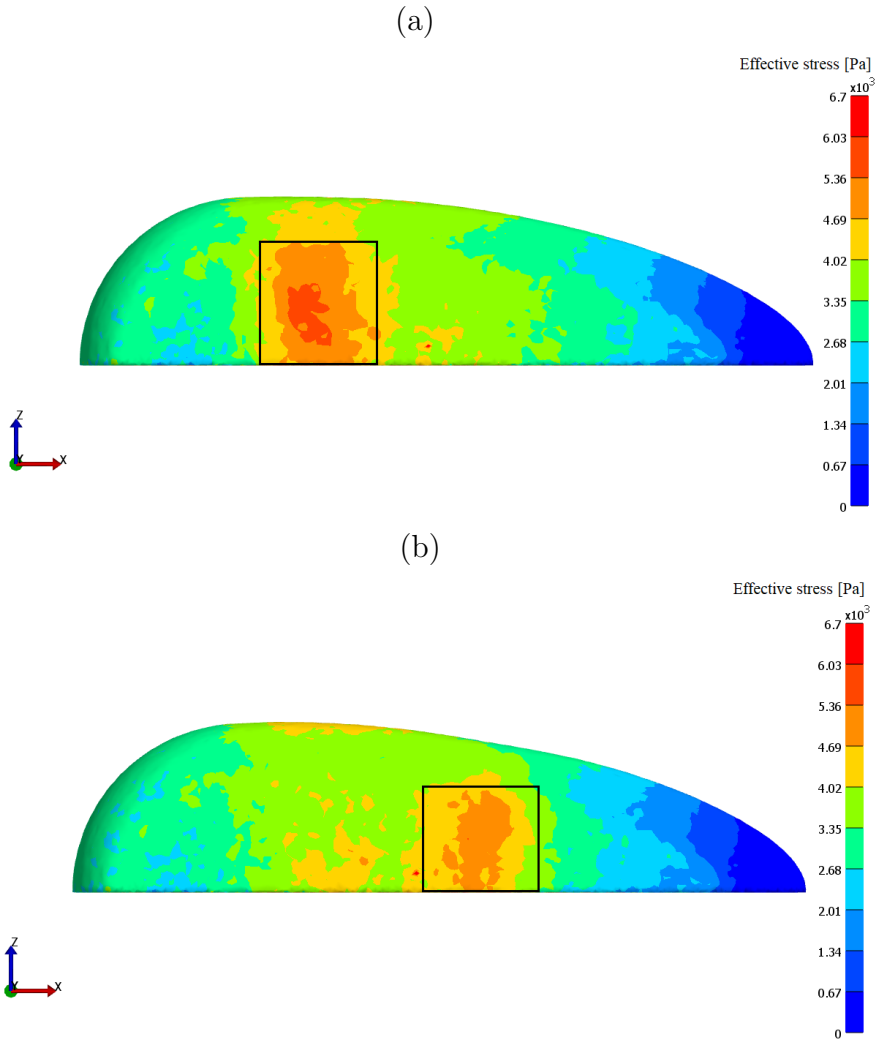


Figure 13: The lesion had a diameter of 15 mm and was 30 times stiffer than the surrounding tissue. The square outlines the 3x3 cm patch centered on the lesion. Viewed from the top. (a) The breast phantom model with lesion located 20 mm to the left along the chest wall. (b) The breast phantom model with lesion located 20 mm to the right along the chest wall.

## 5.5 Effect of the location of the lesion in the orthogonal directions to the compression plates

When the lesion was placed 20 mm towards the compression plate, there was a local maximum of stress at its location. The border between the local maximum and the rest of the breast was sharp. The average of the 3x3 cm square at the local maximum was 4420 Pa and the average over the breast was 4196 Pa, see figure 14a.

For when the lesion was placed 20 mm in negative y-direction (closer to the breast support), there was a local maximum in the middle but not as sharp as in the case with the lesion moved towards the top. The average maximum stress was 4672 Pa and the average stress over the breast being 4194 Pa, see table 2 and figure 14b.



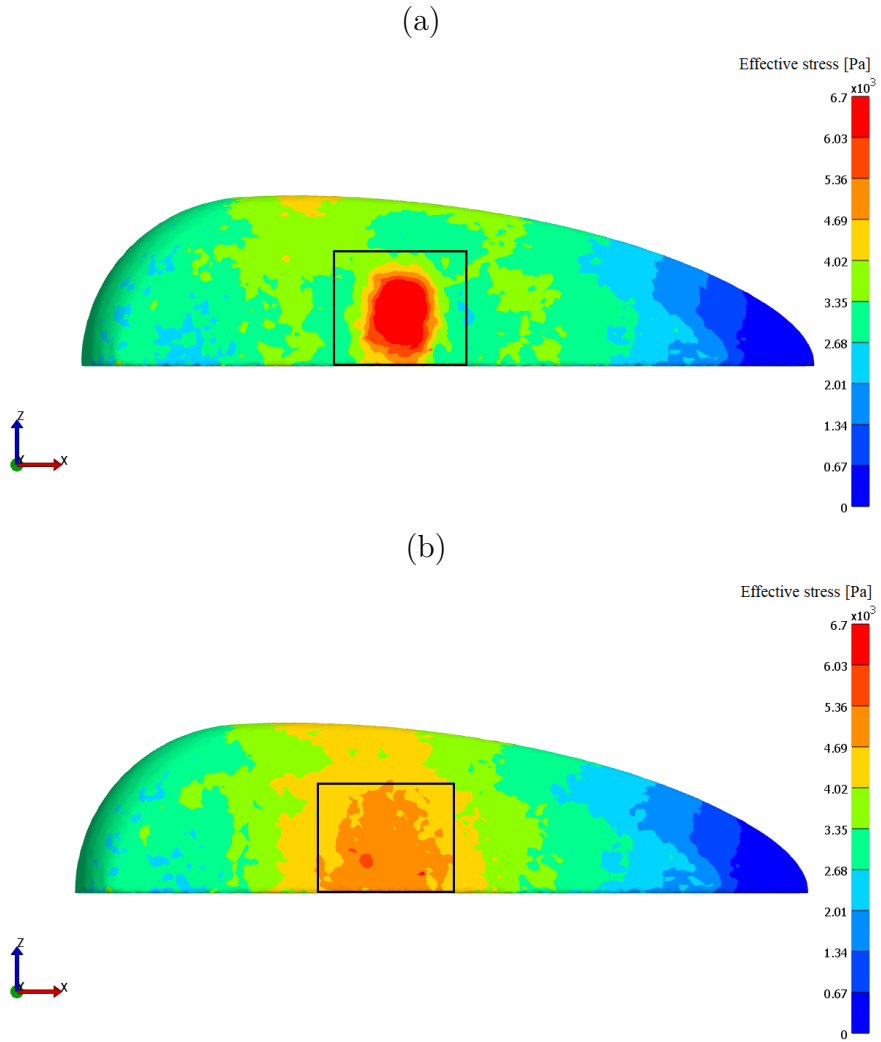


Figure 14: The lesion had a diameter of 15 mm and was 30 times stiffer than the rest of the breast. The square outlines the 3x3 cm patch centered on the lesion. Viewed from the top. (a) The breast phantom model with a lesion located 20 mm towards the compression plate. (b) The breast phantom model with lesion located 20 mm closer to the breast support.

Table 2: Table of overall average stress, local maximum of the breast phantom (3x3 cm average) and the relative increase. The relative increase is the ratio between the average stress at local maximum and the overall average stress in the breast.

	Overall average stress (Pa)	Average stress at local maximum (Pa)	Relative increase (%)
Lesion stiffness x1	4141	4082	-1
Lesion stiffness x50	4294	4860	13
Lesion size 15 mm	4765	5284	11
Lesion size 22 mm	4361	6412	47
Lesion left	4236	4771	13
Lesion right	4198	4497	7
Lesion up	4196	4420	5
Lesion down	4194	4672	11

## 6 Discussion

The aim of the thesis was to introduce mechanical imaging to the *OpenVCT* software platform as well as investigate the change in stress at the breast surface when the stiffness, size and location of a lesion was varied. The breast phantom was remeshed and the boundary conditions were changed during the thesis work. The results regarding the breast phantom (5.2-5.5) were with the new mesh and new boundary conditions.

The results had the expected behaviour in terms of a lesion causing an area of relatively high stress when the breast is compressed (Förnvik et al., 2013). This was shown both in the "proof-of-principle" examples and for all examples with a lesion inside the breast model, see table 2 and figure 15.

The increase in stress level at the area of local high stress was for most of the examples between 11 and 13%. The example with the highest difference in maximum effective stress was when the lesion was 22 mm in diameter, which resulted in an increase of 47%. The smallest difference was an increase of 5% which was the example where the lesion was placed 20 mm up towards the compression plate, see figure 14a. Despite having a sharp border between the area of local high stress, one could expect the average stress around the local high stress to be higher than what is shown in table 2.

This could be explained by the fact that the average stress over the local maximum was taken over a 3x3 cm area, not only localized to the values of highest stress. As the border between the local maximum and the rest of the breast is quite sharp, and the area of local high stress is relatively small, this lowers the average of the region. For the examples where the area of local high stress was greater, there was generally higher stress.

The mean pressure over the pressurized area of the breast at full compression as reported by Dustler et al. (2012) was  $5.6 \pm 2$  kPa. By "the pressurized area" it refers to the area on the pressure sensors that had a stress value above zero.

While the overall average stress for the breast phantom is within this range, it is on the lower side of the range. A possible explanation for this could be that the breast phantom consists entirely of fat which does not increase in stiffness as pressure is applied (Krouskop et al., 1998). This giving an overall lower stress in the breast.

Moreover, the reason for the higher value in Dustler's study (2017) were for some women the pressure of the juxta-thoracic region were measured as well, which gave rise to higher pressure. In the breast model of this thesis, considering it consists only of the breast itself and does not have a chest wall, could explain why the average stress in the model is lower.

Another study by Föörnvik et al. (2013) reported the mean average pressure over the breast to be  $3.4 \pm 1.6$  kPa. This range would be closer to the results in this report. However in the same study, the stress reported for regions with tumours was  $6.8 \pm 5.3$  kPa which is significantly higher average than for most examples in this report.

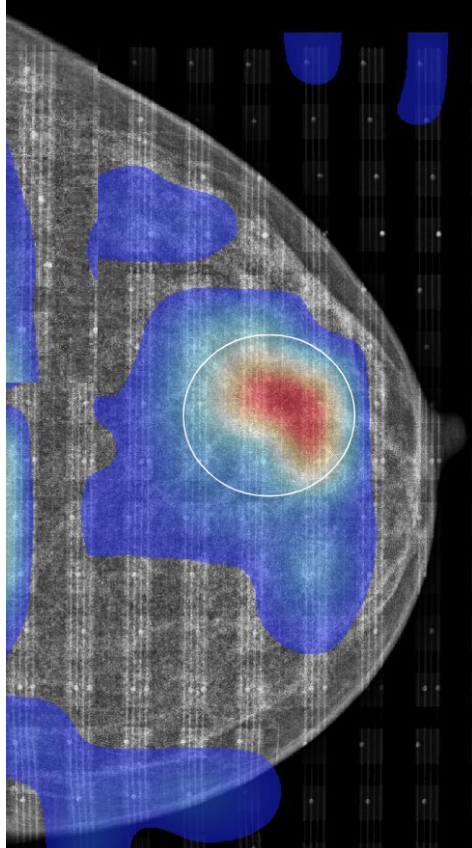


Figure 15: Stress map of invasive ductal carcinoma. The location of the lesion is indicated by the white circle. The colour scale goes from blue (low stress) to red (high stress). Adapted from Dustler.

## 6.1 Limitations

In order to get as reasonable results as possible, values of Young's modulus as published in literature for invasive ductal carcinoma was selected. The values chosen, for example a Young's modulus of 382500 Pa was within the range as reported by Krouskop et al. (1998) at a compression of the tumour by 20%.

However, there is a wide variety of Young's modulus reported for tumour tissue. In another study by Wellman et al. (1999) it was discovered that at 15% strain the tumour could be 70 times stiffer than fat tissue. Also reported by Sarazayan et al. (1995) for invasive ductal carcinomas were that they could be 13 times stiffer than either fat or fibroglandular tissue. The difference in results could possibly be differences in pre-compression as well how the samples have been prepared.

This variety of possible Young's modulus for tumours makes it difficult to choose an appropriate value, which will in turn affect the results.

Another limitation is the narrow size range of the lesions. The size of the lesion was either 10, 15 or 22 mm in diameter. As mentioned in "4.4 Evaluation of lesions", lesions that were smaller than 10 mm in diameter were not able to be detected from the top surface pressure of the breast. This suggests that this might be the size limit for what is currently detectable using the simulated breast phantom. However, changing the stiffness and location of the small lesion could impact how well it is seen on the top surface of the breast.

Another limitation is that the breast phantom consists only of fat tissue. This is not realistic as skin, fibroglandular tissue, and glandular tissue, would be present as well.

If denser tissue like fibroglandular tissue or glandular tissue had been introduced into the model, it would be expected that the average stress of the model would have been higher. This is because fibroglandular and glandular tissue are stiffer than fat and that their Young's modulus increase with increasing strain (Sarvazyan et al., 1995).

Also, considering our model consists only of fat which does not

change significantly in stiffness as more strain is applied (Krouskop et al., 1998), it could be argued that the breast model makes it easier for tumours to be discovered than in a real breast. As reported by Barr and Zhang (2012), it was found that higher compression (40%) made tumours harder to detect as the average stress of the breast increased as well.

Another factor is that the model is devoid of skin. In a study by Vogel (1987) the skin around the chest region was estimated to be around 2 mm in thickness. At this thickness it had an elastic modulus of 0.2 - 3 MPa and a tensile strength of roughly 20 MPa. The failure strain was 60-70 %. Given the high elastic modulus as well as tensile strength, if skin had been introduced into the model the breast would most likely have not deformed as much as when consisting only of fat. Also higher stress over the breast would have been expected as the breast was compressed.

Apart from the material properties chosen for both the breast and the lesion, the boundary conditions chosen will naturally affect the behaviour of the simulated model. For example, when the breast phantom's nodes at the top surface of the breast was restricted in the x-direction this resulted in the same behaviour as if a part of the breast would be fixed to the upper compression plate and other parts not. In figure 9 it is seen that this resulted in local values of high stress at the location where the breast went from fixed to not fixed. No local increase in stress was expected for the model as seen in figure 9 as the breast consisted only of fat and had no lesions.

When changing the boundary to instead have no restriction in the x-direction between the upper plate and the breast, sliding behaviour instead was seen. Also the local high stresses were no longer there, compare figure 9 with figure 11a. However, in reality we would expect the result to be somewhere in between these cases. There would most likely be sliding behaviour for some nodes and friction for other nodes when in contact with the plate.

The chosen mesh for the model will also bring its own set of limitations. It is known that with a finer mesh, the accuracy of the model

will increase (Ottosen and Petersson 1992, p. 2). The drawback is that with more elements, the simulation time increases.

Considering the *OpenVCT* pipeline's main strength is its speed with which it can run its simulations (Bakic et al., 2018a), one would have to weigh the potential increase in accuracy for the speed it takes to complete.

In order to have yet better resolution on the surface of the breast, the elements around the surface would need to be smaller. During the course of the project, different meshing options of the breast model was tried.

Apart from the remeshing as described in "5.3 Changing the mesh and boundary conditions", it was also tried to change the maximum element size of the surface mesh from 5 mm to 4 mm. The simulation time went from around 20 minutes to 46 minutes. It could be argued that such a drastic increase in simulation time compared to the simulation time that the current breast phantom in *OpenVCT* has (around 10 minutes) for the deformation step, would increase the simulation to the point where speed is no longer *OpenVCT*'s clear advantage.

## 6.2 Clinical implementation and ethical aspects

Implementing mechanical imaging into mammography screening and using it as a complement to the X-ray images could aid radiologists in determining whether a tumour is benign or not. Most likely the "Relative Mean Pressure on lesion Area" (RMPA) would be used as in Dustler's study (2017). The RMPA is the pressure on the lesion area relative to the pressure over the entire breast. There would be a lower RMPA value for benign tumours than for malign tumours, considering benign tumours are softer than malignant tumours (Waltz et al., 1996).

The implementation could in turn reduce the amount of women who are recalled from mammography screening. Recalls are done for various reasons, one of the reasons being that a tumour has been found but it is unclear whether it is malignant or not. Unfortunately,



roughly 80-90% of women who are recalled are healthy ie. they either have benign lesions (cysts, fibroadenoma, etc.) or have no lesions at all (Domingo et al., 2016). Women who have been recalled have reported to feel anxious and have experienced both long- and short term psychosocial consequences (Bolejko et al., 2015). By Dustler et al. (2017), it was estimated that if mechanical imaging was to be implemented clinically, there could be a possible 36% reduction in recall rates.

From an ethical point of view, implementing mechanical imaging could spare women unnecessary anxiety because of this potential reduction in recall rates. Moreover, since mechanical imaging does not use any form of radiation it would most likely be easier to implement clinically from an ethical standpoint than an imaging method which uses radiation.

### **6.3 Future work**

For future work using a hyperelastic material model instead of linear elastic would increase the breast phantom's realism. With a hyperelastic model we would expect higher stress values overall, especially at the location of a lesion.

Moreover, implementing more tissue types into the FE-model of the breast phantom would increase the realism as well. This could be done by using the voxel values of the *OpenVCT* which code for the different tissue in the breast phantom, and map this onto the mesh of the breast phantom.

Adding variation of tissue types in the FE-breast model would enable to investigate the effect background tissue has on the MI data and could also help in optimizing MI acquisition parameters.

In the further future a mechanical model for tumour growth could be implemented and the resulting surface stress map of the breast studied in order to detect growing tumours.

## 7 Conclusion

To conclude, with a higher stiffness of the lesion there was an area of local high stress at the top surface of the breast. The same behaviour was seen when the lesion was increased in size and its location altered. These results were similar to known clinical data of mechanical imaging in mammography. In other words, implementing mechanical imaging into the *OpenVCT* software platform was successful.

However, for most examples the increase in stress at the location of the lesion was relatively small. This could be attributed by the fact that the breast model consists entirely of fat which does not get significantly stiffer with increasing strain. This would be need to investigated be further in future studies.

## References

- Andersson I., Hildell J., Mühlow A., Pettersson H. 1978. *Number of projections in mammography: influence on detection of breast disease*. AJR Am J Roentgenol 130(2): 349-351.
- Bakic P.R. Barufaldi B., Pokrajac D. Weinstein Maidment A.D.A. 2018. *Optimized simulation of breast anatomy for virtual clinical trials*. Proc. SPIE 10718. 14th International Workshop on Breast Imaging (IWBI 2018)
- Bakic P.R. Maidment A.D.A. 2012. *Digital Phantoms for Breast Imaging*. In: Markey MK, ed. Physics of Mammographic Imaging. Philadelphia, PA: Taylor Francis.
- Bakic P. R., Pokrajac D. D., De Caro R., Maidment A.D.A. 2014. *Realistic Simulation of Breast Tissue Microstructure in Software Anthropomorphic Phantoms*. International Workshop on Breast Imaging (IWDM): pp. 348-55. Gifu, Japan.
- Barufaldi B., Higginbotham D., Bakic P.R., Maidment A.D. *Open-VCT: A GPU-Accelerated Virtual Clinical Trial Pipeline for Mammography and Digital Breast Tomosynthesis*. 2018. Physics of Medical Imaging: SPIE.
- Barr R.G., Zhang Z. 2012. *Effects of precompression on elasticity imaging of the breast: development of a clinically useful semiquantitative method of precompression assessment*. J. Ultrasound Med 31: 895–902
- Belaid N., Cespedes I., Thijssen J. and Ophir J. 1994. *Lesion detection in elastography versus echography: a quantitative analysis*. Ultrasound Med. Bioi. 20: 877-891.
- Bolejko A., Hagell P., Wann-Hansson C., and Zackrisson S. 2015. *Prevalence, Long-term Development, and Predictors of Psychosocial*

*Consequences of False-Positive Mammography among Women Attending Population-Based Screening.* Cancer Epidemiology Biomarkers Prevention 24 (9): 1388-1397

Bröstcancerfonden. 2020. <https://brostcancerforbundet.se/ombrostcancer/>

Curry T., Dowdey J., and Murry R. 1990. *Christensen's Physics of Diagnostic Radiology.* Lea Febiger. p 50.

Diaz O. Personal correspondence.

Diekmann F., Meyer H., Diekmann S., Puong, S., Muller S., Bick U., and Rogalla P. 2009. *Thick slices from tomosynthesis data sets: Phantom study for the evaluation of different algorithms.* Journal of Digital Imaging, 22(5):519–526.

Domingo L., Hofvind S., Hubbard R.A, Roman M., Benkeser D., Sala M. and Castells X. 2016. *Cross-national Comparison of Screening Mammography Accuracy Measures in U.S., Norway, and Spain.* Eur Radiology (8): 2520 - 2528

Dustler. Personal correspondence.

Dustler M., Andersson I., Brorson H., Fröjd P., Mattsson S., Tingberg A., Zackrisson S., Förnvik D. 2012. *Breast compression in mammography: pressure distribution patterns.* Acta Radiologica 53 (9): 973-980

Dustler M., Förnvik D., Timberg P., Andersson I., Petersson H., Brorson H., Tingberg A., and Zackrisson S. 2017. *Can mechanical imaging increase the specificity of mammography screening?* European Radiology 27 (8): 3217-3225

Fang Q. and Boas D. *Tetrahedral mesh generation from volumetric binary and gray-scale images.* 2009. Proceedings of IEEE International Symposium on Biomedical Imaging, pp. 1142-1145

FEBio. <http://www.febio.org>

Finlayson C. A., MacDermott T. A. 2000. *Ultrasound Can Estimate the Pathologic Size of Infiltrating Ductal Carcinoma*. Arch Surg. 135: 158-159.

Ford H. 1963. *advanced mechanics of materials*. Longmans. London.

Fung Y.C. 1993. *Biomechanics: mechanical properties of living tissues*. Springer, New York

Förnvik D., Andersson I., Dustler M., Ehrnström R., Rydén L., Tingberg A., Zackrisson S., Aaltonen K. 2013. *No evidence for shedding of circulating tumor cells to the peripheral venous blood as a result of mammographic breast compression*. Breast Cancer Res Treat 141: 187–195.

Garra B. S., Cespedes I., Ophir J., Spratt S. et al. 1997. *Elastography of breast lesions: initial clinical results*. Radiology 202: 79-86.

Gefen A., Dilmoney B. 2007. *Mechanics of the normal woman's breast*. Technol Health Care 15(4):259–271

Gotzsche P. C., Jorgensen K. J. 2013. *Screening for breast cancer with mammography*. Cochrane Database Syst Rev CD001877.

Gotzsche P. C., Jorgensen K. J. 2013. *The benefits and harms of breast cancer screening*. Lancet 381: 799.

Han L., Hipwell J., Tanner C., Taylor Z., Mertzaniidou T., Cardoso J., et al. 2012. *Development of patient-specific biomechanical models for predicting large breast deformation*. Phys. Med. Biol. 57: 455–472.

Hricak H., Choyke P. L., Eberhardt S. C., Leibel S. A., Scardino P. T. 2007. *Imaging prostate cancer: a multidisciplinary perspective* [published correction appears in Radiology. 2007 Oct;245(1):302]. Radiology 243(1): 28-53.

- Kim S.J., Moon W.K., Cho N., Cha J.H., Kim S.M., Im J.G. 2006. *Computer-aided detection in digital mammography: comparison of craniocaudal, mediolateral oblique, and mediolateral views*. Radiology 241(3): 695-701.
- Krouskop T.A., Wheeler T.M., Kallel F., Garra B.S., Hall T. 1998. *Elastic moduli of breast and prostate tissues under compression*. Ultrason Imaging 20(4): 260-274.
- Lago M., Maidment A.D.A., Bakic P.R.. 2013. *Modelling of mammographic compression of antropomorphic software breast phantom using FEBio*. Proceedings of the 11th International Symposium. Computer Methods in Biomechanics and Biomedical Engineering. Salt Lake City, Utah, USA
- Maidment A. D. A. 2014. *Virtual Clinical Trials for the Assessment of Novel Breast Screening Modalities*. Proceedings of 12th International Workshop on Breast Imaging (IWDM). Gifu, Japan: Springer: pp. 1-8.
- Ophir J., Cespedes I., Garra B., Ponnekanti H., Huang Y. and Maklad N. 1996. *Elastography: ultrasonic imaging of tissue strain and elastic modulus in vivo*. Eur. J. Ultrasound 1: 49-70.
- Ottosen N. S., and Petersson H. 1992. *Introduction to the finite element method*. Prentice Hall Europe.
- Pokrajac D. D., Maidment A. D. A., Bakic P. R. *Optimized generation of high resolution breast anthropomorphic software phantoms*. 2012. Medical Physics 39(4): 2290-302.
- Ramiao N., Martins P., Rynkevic R., Fernandes A., Barroso M., Santos D. 2016. *Biomechanical properties of breast tissue, a state-of-the-art review*. Biomechanics and Modeling in Mechanobiology 15: 1307-1323.

- Sarvazyan A. Egorov V. 2009. *Mechanical Imaging in Medical Applications*. Proceeding of Annual International Conference of the IEEE Engineering in Medicine and Biology Society. IEEE Engineering in Medicine and Biology Society. pp. 1975-8.
- Sarvazyan A. 1993. *Shear acoustic properties of soft biological tissues in medical diagnostics*. Journal of The Acoustical Society of America 93: 2329-2330.
- Stewart B. W., Wild C. P. 2014. *World Cancer Report*. International Agency for Research on Cancer (IARC). ISBN 978-92-832-0429-9.
- Ståhle P. 2015. *Introduktion till hållfasthetsläran: Lärobok, övningar, anvisningar och facit*. Lund.
- Sweeney R. I., Lewis S. J., Hogg P., McEntee M. F. 2018. *A review of mammographic positioning image quality criteria for the craniocaudal projection*. The British journal of radiology, 91(1082), 20170611.
- Vieira M. A. C., Bakic P. R., and Maidment, A.D.A. 2013. *Effect of denoising on the quality of reconstructed images in digital breast tomosynthesis*. In Proceedings of SPIE 8668: 56.
- Vogel H.G. 1987. *Age Dependence of Mechanical and Biochemical Properties of Human Skin. Part I: Stress-Strain Experiments, Skin Thickness and Biochemical Analysis*. Bioengineering and the Skin 3: 67-91.
- Vorrherr H. 1974. *The Breast: Morphology, Physiology, and Lactation* Academic Press. New York, London.
- Young S., Bakic P. R., Myers K.J., Jennings R.J., and Park S. 2013. *A virtual trial framework for quantifying the detectability of masses in breast tomosynthesis projection data*. Medical Physics, 40(5): 56.
- Walz M., Teubner J., and Georgi, M. 1993. *Elasticity of benign and malignant breast lesions imaging, Application and results in clinical*

*and general practice.* Abstr. Eight Intern.Congo Ultrasonic Exam.  
Breast, 56.



# Appendix

## MATLAB script "lesion.m"

```
1 clear all
2
3 %Load in information of the mesh. Both elements
  and nodes
4 mesh = 'C:\Users\Rebecca\Documents\Rebeccasmapp\
  Master Thesis\Test';
5 [nodes, elements]=loadAbaqusInput(['mesh '.inp'],30)
  ;
6
7 %Origin of the lesion
8 x0 = 70;
9 y0 = 40;
10 z0 = 11;
11
12 %Coordinates
13 x1 = nodes(:,1);
14 y1 = nodes(:,2);
15 z1 = nodes(:,3);
16
17 %Radius of the lesion
18 r = 7.5;
19
20 %Number of nodes for the entire mesh
21 nmbr_nodes = size(nodes,1);
22
23 %Number of elements for the entire mesh
24 nmbr_elements = size(elements,1);
25
26 %Which node has the correct distance to the origin
27 node_within_circle = zeros(nmbr_nodes,1);
```

```

28
29 for i = 1:nmbr_nodes
30 dist = sqrt((x1(i) - x0).^2 + (y1(i) - y0).^2 + (
      z1(i) - z0).^2);
31 if(dist <= r)
32     node_within_circle(i,1) = 1;
33 end
34 end
35
36 %Visualizing the selected nodes in the mesh
37 figure (); scatter3(x1,y1,z1)
38 hold on
39 scatter3(x1(node_within_circle==1),y1(
      node_within_circle==1),z1(node_within_circle
      ==1),'.')
40
41 %The node number of the nodes making up the lesion
42 nmbr_node_within_circle = find(node_within_circle)
      ;
43 elements_nodes = zeros(nmbr_elements,4);
44
45 %Locating which nodes belong to which element. If
      an element has a
46 %”selected node” in it, place a 1 at this position
47 for j = 1:size(elements_nodes,2)
48     for k = 1:size(nmbr_node_within_circle,1)
49         for m = 1:nmbr_elements
50             if(elements(m,j) == nmbr_node_within_circle(k
      ,1))
51                 elements_nodes(m,j) = 1;
52             end
53         end
54     end
55 end

```

```

56
57 %Check to see how many nodes belong to an element.
   A minimum of belonging nodes will be 4 (all of
   them)
58 sum = sum(elements_nodes,2);
59 belonging_elements = find(sum == 4);

```

## **MATLAB script "Onemesh.m"**

```

1 %Script to locate elements in .feb file and change
   the material properties
2 %of the lesion elements
3
4 %Read in .feb file of breast with homogenous
   material properties (no lesion)
5 fidXML=fopen( 'C:\Users\Rebecca\Documents\
   Rebeccasmapp\Master Thesis\Test.feb', 'r' );
6 %New .feb file to write new material properties
   into
7 fidXMLnew=fopen( 'C:\Users\Rebecca\Documents\
   Rebeccasmapp\Master Thesis\Test_lesion.feb', 'w'
   );
8
9   d = 0;
10  k = 1;
11  first_index = num2str(belonging_elements(1,1))
   ;
12  while( d == 0 )
13      line=fgetl(fidXML);
14      lineNew = line;
15      if (k < size(belonging_elements,1) &&
   contains(lineNew, [ '<tet4 id='
   first_index ''' ] ) == 1)
16          lineNew = line;
17          if belonging_elements(k,1) < 1000

```

```

18         lineNew(33) = "2";
19     end
20     if belonging_elements(k,1) >= 1000 &&
        belonging_elements(k,1) < 10000
21         lineNew(34) = "2";
22     end
23     if belonging_elements(k,1) >= 10000 &&
        belonging_elements(k,1) < 100000
24         lineNew(35) = "2";
25     end
26     if belonging_elements(k,1) >= 100000
27         lineNew(36) = "2";
28     end
29     fprintf(fidXMLnew, [lineNew, '\r\n']);
30     k = k+1;
31     first_index = num2str(
        belonging_elements(k,1));
32     else
33         fprintf(fidXMLnew, [lineNew, '\r\n'
34         ]);
35     end
36     if contains(lineNew, '</febio_spec>') == 1
37         d = 1;
38     end
39
40 end
41
42 fclose(fidXML);
43 fclose(fidXMLnew);

```